Astroparticle Physics 34 (2011) 327–332

Contents lists available at ScienceDirect

Astroparticle Physics

journal homepage: www.elsevier.com/locate/astropart

Review

Automatic Alignment system during the second science run of the Virgo interferometer

T. Accadia [u], F. Acernese [f,h], F. Antonucci [n], P. Astone [n], G. Ballardin [b], F. Barone [f,h], M. Barsuglia [a], A. Basti [k,l], Th.S. Bauer [w], M.G. Beker [w], A. Belletoile [u], S. Birindelli [y], M. Bitossi [k], M.A. Bizouard [s], M. Blom [w], F. Bondu [z], L. Bonelli [k,l], R. Bonnand [v], V. Boschi [k], L. Bosi [i], B. Bouhou [a], S. Braccini [k], C. Bradaschia [k], A. Brillet [y], V. Brisson [s], R. Budzyński [af], T. Bulik [ag,ah], H.J. Bulten [w,x], D. Buskulic [u], C. Buy [a], G. Cagnoli [c], E. Calloni [f,g], E. Campagna [c,d], B. Canuel [b], F. Carbognani [b], F. Cavalier [s], R. Cavalieri [b], G. Cella [k], E. Cesarini [d], O. Chaibi [y], E. Chassande-Mottin [a], A. Chincarini [e], F. Cleva [y], E. Coccia [p,q], C.N. Colacino [k,l], J. Colas [b], A. Colla [n,o], M. Colombini [o], A. Corsi [n], J.-P. Coulon [y], E. Cuoco [b], S. D'Antonio [p], V. Dattilo [b], M. Davier [s], R. Day [b], R. De Rosa [f,g], G. Debreczeni [al], M. del Prete [k,m], L. Di Fiore [f], A. Di Lieto [k,l], M. Di Paolo Emilio [p,r], A. Di Virgilio [k], A. Dietz [u], M. Drago [ac,ad], V. Fafone [p,q], I. Ferrante [k,l], F. Fidecaro [k,l], I. Fiori [b], R. Flaminio [v], L.A. Forte [f], J.-D. Fournier [y], J. Franc [v], S. Frasca [n,o], F. Frasconi [k], A. Freise [am], M. Galimberti [v], L. Gammaitoni [i,j], F. Garufi [f,g], M.E. Gáspár [al], G. Gemme [e], E. Genin [b], A. Gennai [k], A. Giazotto [k], R. Gouaty [u], M. Granata [a], C. Greverie [y], G.M. Guidi [c,d], J.-F. Hayau [z], H. Heitmann [y,z], P. Hello [s], S. Hild [an], D. Huet [b], P. Jaranowski [ai], I. Kowalska [ag], A. Królak [ae,aj], N. Leroy [s], N. Letendre [u], T.G.F. Li [w], N. Liguori [aa,ab], M. Lorenzini [c], V. Loriette [t], G. Losurdo [c], E. Majorana [n], I. Maksimovic [t], N. Man [y], M. Mantovani [k,m,*], F. Marchesoni [i], F. Marion [u], J. Marque [b], F. Martelli [c,d], A. Masserot [u], C. Michel [v], L. Milano [f,g], Y. Minenkov [p], M. Mohan [b], N. Morgado [v], A. Morgia [p,q], S. Mosca [f,g], V. Moscatelli [n], B. Mours [u], I. Neri [i,j], F. Nocera [b], G. Pagliaroli [p,r], L. Palladino [p,r], C. Palomba [n], F. Paoletti [b,k], S. Pardi [f,g], M. Parisi [g], A. Pasqualetti [b], R. Passaquieti [k,l], D. Passuello [k], G. Persichetti [f,g], M. Pichot [y], F. Piergiovanni [c,d], M. Pietka [ai], L. Pinard [v], R. Poggiani [k,l], M. Prato [e], G.A. Prodi [aa,ab], M. Punturo [i], P. Puppo [n], D.S. Rabeling [w,x], I. Rácz [al], P. Rapagnani [n,o], V. Re [p,q], T. Regimbau [y], F. Ricci [n,o], F. Robinet [s], A. Rocchi [p], L. Rolland [u], R. Romano [f,h], D. Rosińska [ak], P. Ruggi [b], B. Sassolas [v], D. Sentenac [b], L. Sperandio [p,q], R. Sturani [c,d], B. Swinkels [b], A. Toncelli [k,l], M. Tonelli [k,l], O. Torre [k,l], E. Tournefier [u], F. Travasso [i,j], G. Vajente [k,l], J.F.J. van den Brand [w,x], S. van der Putten [w], M. Vasuth [al], M. Vavoulidis [s], G. Vedovato [ac], D. Verkindt [u], F. Vetrano [c,d], A. Viceré [c,d], J.-Y. Vinet [y], H. Vocca [i], R.L. Ward [a], M. Was [s], M. Yvert [u]

[a] *Laboratoire AstroParticule et Cosmologie (APC), Université Paris Diderot, CNRS: IN2P3, CEA: DSM/IRFU, Observatoire de Paris 10, rue A. Domon et L. Duquet, 75013 Paris, France*
[b] *European Gravitational Observatory (EGO), I-56021 Cascina (PI), Italy*
[c] *INFN, Sezione di Firenze, I-50019 Sesto Fiorentino, Italy*
[d] *Università degli Studi di Urbino 'Carlo Bo', I-61029 Urbino, Italy*
[e] *INFN, Sezione di Genova, I-16146 Genova, Italy*
[f] *INFN, Sezione di Napoli, Complesso Universitario di Monte S. Angelo, I-80126 Napoli, Italy*
[g] *Università di Napoli 'Federico II', Complesso Universitario di Monte S. Angelo, I-80126 Napoli, Italy*
[h] *Università di Salerno, Fisciano, I-84084 Salerno, Italy*
[i] *INFN, Sezione di Perugia, I-06123 Perugia, Italy*
[j] *Università di Perugia, I-06123 Perugia, Italy*
[k] *INFN, Sezione di Pisa, I-56127 Pisa, Italy*
[l] *Università di Pisa, I-56127 Pisa, Italy*
[m] *Università di Siena, I-53100 Siena, Italy*
[n] *INFN, Sezione di Roma, I-00185 Roma, Italy*
[o] *Università 'La Sapienza', I-00185 Roma, Italy*
[p] *INFN, Sezione di Roma Tor Vergata, I-00133 Roma, Italy*
[q] *Università di Roma Tor Vergata, I-00133 Roma, Italy*
[r] *Università dell'Aquila, I-67100 L'Aquila, Italy*
[s] *LAL, Université Paris-Sud, IN2P3/CNRS, F-91898 Orsay, France*
[t] *ESPCI, CNRS, F-75005 Paris, France*
[u] *Laboratoire d'Annecy-le-Vieux de Physique des Particules (LAPP), Université de Savoie, CNRS/IN2P3, F-74941 Annecy-Le-Vieux, France*
[v] *Laboratoire des Matériaux Avancés (LMA), IN2P3/CNRS, F-69622 Villeurbanne, Lyon, France*
[w] *Nikhef, National Institute for Subatomic Physics, P.O. Box 41882, 1009 DB Amsterdam, The Netherlands*
[x] *VU University Amsterdam, De Boelelaan 1081, 1081 HV Amsterdam, The Netherlands*

0927-6505/$ - see front matter
doi:10.1016/j.astropartphys.2010.10.005

[y] Université Nice-Sophia-Antipolis, CNRS, Observatoire de la Côte d'Azur, F-06304 Nice, France
[z] Institut de Physique de Rennes, CNRS, Université de Rennes 1, 35042 Rennes, France
[aa] INFN, Gruppo Collegato di Trento, I-38050 Povo, Trento, Italy
[ab] Università di Trento, I-38050 Povo, Trento, Italy
[ac] INFN, Sezione di Padova, I-35131 Padova, Italy
[ad] Università di Padova, I-35131 Padova, Italy
[ae] IM-PAN, 00-956 Warsaw, Poland
[af] Warsaw University, 00-681 Warsaw, Poland
[ag] Astronomical Observatory Warsaw University, 00-478 Warsaw, Poland
[ah] CAMK-PAN, 00-716 Warsaw, Poland
[ai] Białystok University, 15-424 Białystok, Poland
[aj] IPJ, 05-400 Świerk-Otwock, Poland
[ak] Institute of Astronomy, 65-265 Zielona Góra, Poland
[al] RMKI, H-1121 Budapest, Konkoly Thege Miklós út 29-33, Hungary
[am] University of Birmingham, Birmingham B15 2TT, United Kingdom
[an] University of Glasgow, Glasgow G12 8QQ, United Kingdom

ARTICLE INFO

Article history:
Received 2 July 2010
Received in revised form 28 September 2010
Accepted 12 October 2010
Available online 23 October 2010

Keywords:
Gravitational wave detectors
Interferometry
Control systems
Angular control
Alignment

ABSTRACT

In this paper the performances of the Automatic Alignment sensing and control system in the Virgo gravitational wave detector, during the second scientific run from July 7th 2009 to January 8th 2010, are described. The accuracy of the angular control loops fulfills the original Virgo requirements, reaching the accuracy of a few nano-radians for the most critical angular degrees of freedom, and the control noise is below the Virgo design sensitivity in the whole detection band.

Contents

1. The Virgo gravitational wave detector

The Virgo interferometer [1] is a ground based gravitational wave detector consisting of a Michelson interferometer with 3 km long Fabry–Perot cavities in its arms and a power-recycling mirror, see Fig. 1. The main optical elements are fused silica cylinders suspended in ultra-high vacuum by a seismic isolation system, *super-attenuators* [2]. This suspension system provides an excellent seismic isolation in the frequency range above the resonances of the mechanical system in the vertical and horizontal directions (more than 10 orders of magnitude above a few Hz). The *super-attenuator* is composed of an inverted pendulum, with a very low mechanical resonant frequency, which provides a pre-isolation stage, and a cascade of attenuator filters.

The last stage of the suspension is formed by the *marionette* and the *reference mass*. The marionette, which is a massive element connected to the last vertical isolation stage, supports the reference mass and the mirror and acts on their position by means of four steel wires, in the longitudinal and in the angular degrees of freedom. The reference mass is a cylindrical component which surrounds the mirror and acts on its position by coil-magnet actuators.

The input beam is generated by a system of master/slave lasers with a power of 60 W and a wavelength of 1064 nm. The beam jitter is reduced by passing the input light through a 144 m long *input mode-cleaner* (IMC). The laser beam is split at the *beam splitter* mirror (BS) into two beams which are injected into the two orthogonal Fabry–Perot arm cavities (North and West arms), to enhance the phase shift produced by the optical path length variation of the beam caused by a gravitational wave.

The longitudinal positions of all the mirrors are controlled in such a way that the arm cavities are resonant and the recombination of the beams at the BS creates a destructive interference in the main output port (B1), the asymmetric port, see Fig. 1.

This is the *dark fringe* condition. In this condition almost all the light is reflected back to the power recycling mirror (PR), only a millionth part of the light circulating in the cavities reaches the dark fringe. The presence of this mirror allows to increase the circulating power in the interferometer.

The light coming from the dark port of the interferometer is filtered by an *output mode cleaner* (OMC), before being detected by a set of high-sensitivity photo-diodes at the B1 detection port.

* Corresponding author at: Università di Siena, I-53100 Siena, Italy.
E-mail address: maddalena.mantovani@ego-gw.it (M. Mantovani).

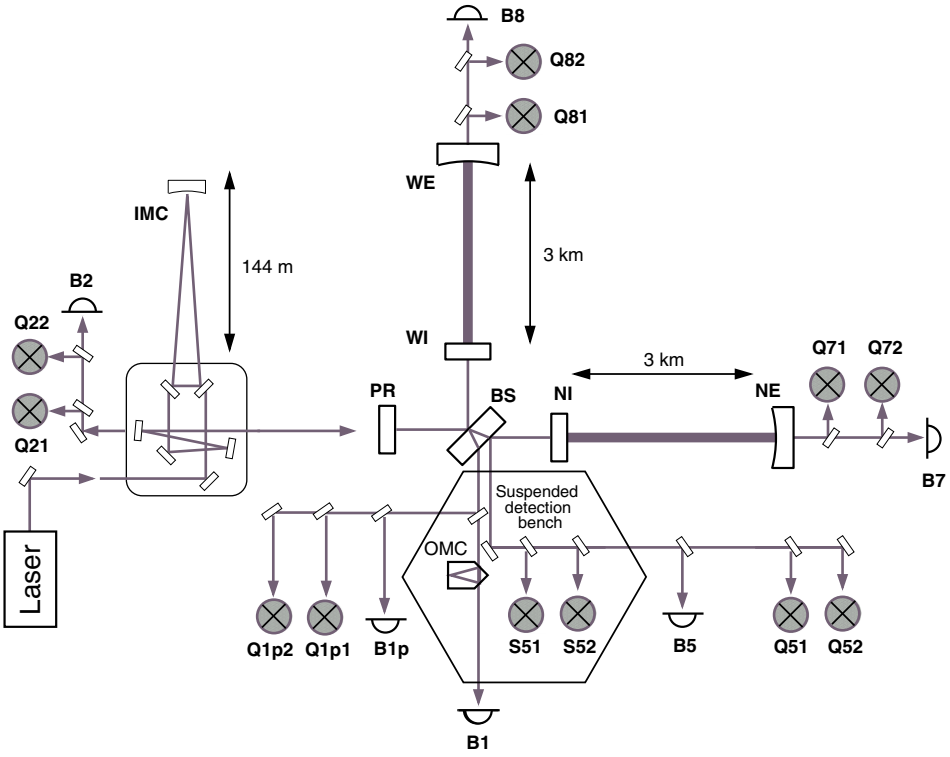

Fig. 1. Simplified scheme of the Virgo optical design. The diodes, placed on external detection benches, used for longitudinal (with names starting with **B**), and angular control (starting with **Q**) are shown. On the suspended detection bench two more quadrant diodes used for angular control (with names starting with **S**) are placed. PR is the power recycling mirror, BS is the beam splitter, NI and NE are the input and end mirrors of the North cavity (equally for the West cavity). IMC and OMC are the input and output mode cleaners, respectively. See main text for details.

2. Angular control system

The detection principle of a gravitational wave interferometer is to sense the passage of a gravitational wave as a change in the intensity of light at the asymmetric port, due to the phase shift in the long arms. This is possible only if the test masses are suspended well enough to be considered as *free-falling test masses*.

These instruments provide an useful signal only when the optical components are positioned precisely at pre-defined locations relative to each other. This set of positions is called the *operating point*. Sophisticated electro-optical feed-back control systems are required to continuously measure and restore the operating point.

A misalignment or a displacement of a mirror produces a variation of the effective arm length of the interferometer which can mimic the effect of a gravitational wave. For this reason two separate systems to control the mirror position are used: one for the longitudinal position along the optical axis (called *Locking*), and the other for the alignment (called *Automatic Alignment*).

In order to reach the design strain sensitivity of Virgo, $h < 3 \times 10^{-21} \Big/ \sqrt{\text{Hz}}$ at 10 Hz, the position of the mirrors has to be actively maintained at the *operating point* with very high accuracy. Tolerable deviations from the operating point along the optical axis are typically of the order of $\sim 10^{-15} - 10^{-12}$ m in the longitudinal direction [3] and $\sim 10^{-1} - 10^{-3}$ μrad of total RMS [4] in the angular directions, while the free motion of the suspended mirrors would be orders of magnitude larger than that: from 10 to 1 μrad in the region between 100 mHz and a few Hz.

Thus the angular control system has to be implemented in order to reduce the mirror misalignments in the frequency region in which the super-attenuator does not fulfill the alignment requirements, below the mechanical resonances (a few Hz).

During the switch-on procedure of the longitudinal control loops (called also *lock*), the angular positions of the main mirrors and of the beam splitter are controlled by using local references (*Local Control* [5], with a stability of some μrad per hour).

The mirror angular positions in data taking mode cannot be controlled by the Local Controls due to the long term drifts of the references and low accuracy of the controls, which spoils the overall alignment, and due to the high electronic/shot noise of the sensors used.

After the lock has been acquired the angular control is switched to a global control system, the *Automatic Alignment*, which uses error signals coming from the interferometer itself with a modulation–demodulation technique.

The Automatic Alignment is a servo-loop system designed to reduce the fluctuations of the mirror angular positions with respect to the beam, to maintain the overall alignment of the optical elements and to reduce the noise at the dark fringe port (the local control sensing noise is more than 10^{-4} μrad$\Big/\sqrt{\text{Hz}}$, as opposed to the global sensing noise of about $10^{-6} - 10^{-7}$ μrad$\Big/\sqrt{\text{Hz}}$).

The Automatic Alignment system controls the angular pitch and yaw[1] misalignments of the seven degrees of freedom, namely the PR, BS, NI, WI, Differential End $\left(\frac{\theta_{\text{WE}} - \theta_{\text{NE}}}{2}\right)$ and Common End $\left(\frac{\theta_{\text{WE}} + \theta_{\text{NE}}}{2}\right)$, and the main input beam (IB). The alignment error signals are extracted using five beams coming out of the interferometer. They are: the main beam reflected by the interferometer (Q2), the two beams transmitted by the long arm cavities (Q7/8), the pick-off beam at the secondary surface of the BS (Q5 for the quadrants in air on the detection bench and S5 for the quadrants suspended in vacuum) and the beam detected in the asymmetric port before the OMC (Q1p). At each detection port two quadrant diodes (*quadrants* for short) are installed at 90° of Gouy phase difference to have

[1] The pitch and yaw directions are defined as the rotation around the horizontal (x) and vertical (y) axis, respectively, where the z axis is defined along the beam.

independent signals, see Fig. 1. These are photo-diodes with four separate elements. Each quadrant diode can provide four signals: the sum over four quadrants gives the same signal as a normal photo-diode. The differences between the upper and lower elements and the left and right elements are computed and give the absolute vertical and horizontal positions of the beam on the diode, *DC signals*. Demodulation of the differential quadrant diode outputs at the modulation frequency yields two additional signals (in-phase and quadrature) that contain information about the angle and position (vertical and horizontal, respectively) of the phase front of the carrier with respect to the sideband, *RF signals*.

3. Automatic Alignment control scheme

The angular control scheme can be described with a block diagram, as it is shown in Fig. 2:

The *Sensing* (**S**) which is formed by the sensing electronics: quadrant diodes and readout electronics, which detect the interferometer beams to extract the informations about mirror misalignments.

The *Control* (**C**) which is formed by the *Control Matrix* and the *Correctors*. The control matrix gives the relation between the set of quadrant signals and the set of mirror tilts; its entries are the low frequency limit, below the cavity pole, of the transfer functions between the angular degrees of freedom and the quadrant signals [6], sampled at 2 kHz.

The angular corrections are constructed by filtering the error signals with properly designed control filters (correctors).

The *Mechanics* (**M**) which corresponds to the Transfer Function from the marionetta, where the angular corrections are applied, to the mirror angular displacement.

The *Optical configuration* (**O**) which represents the interferometer response to the mirror misalignments.

The main sources of noise in the angular control scheme are the *Seismic noise*, n_{seism}, which dominates the error signals below some Hz, and the *Electronics/Shot noise* of the sensing path, $n_{elec/shot}$, which dominates the error signals above 10 Hz. The aim of the Automatic Alignment system is to suppress the seismic displacement of the optics, at low frequency, while cutting off the electronic noise for not reintroducing it in the gravitational wave signal, starting from 10 Hz.

For the Automatic Alignment system two topologies of control have been developed: the *Fast control* and the *Drift control*.

The Fast control uses the global signals with a control bandwidth of a few Hz, where all the local controls are switched off.

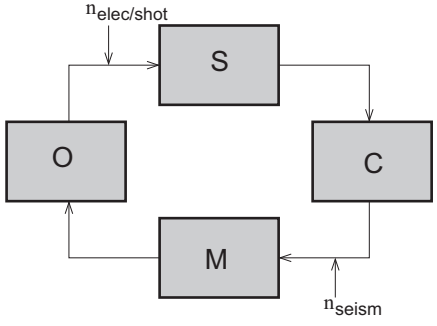

Fig. 2. Blocks scheme for the angular control system. The *Sensing* composed by the readout electronics (quadrant diodes, demodulators and ADC) labeled with **S**; the *Control*, formed by the control matrix and the corrector filters, labeled with **C**; the *Mechanics*, the mechanical transfer function (TF) from the correction injection point and the angular displacement of the optics, labeled whit **M**; and the *Optical configuration*, which takes into account the TF between the mirror angular displacement and the optical signals, labeled with **O**. The main sources of noise in the angular control scheme are the seismic noise n_{seism} and the sensing electronic/shot noise $n_{elec/shot}$.

The Drift control is a mixture of a global and local controls; the overall alignment is kept by a low frequency global control, with a few mHz of bandwidth, while the high frequency control is done by using local references; this avoids the slow independent drifts of the mirrors and allows maintaining a reasonably good global alignment that would not occur with local control alone.

In a perfectly decoupled control system all the angular degrees of freedom should be controlled by a fast control mode, but in reality strong couplings between the degrees of freedom are present. A way to separate them is to implement an hierarchical control engaging the controls with different bandwidths: the dominant degrees of freedom should be engaged with a larger control bandwidth to reduce their influence on the other degrees of freedom (d.o.f.).

Moreover, the choice between fast and drift control depends also on noise issues. For example, if a given d.o.f. has a strong coupling factor to the dark fringe, it is necessary to engage it with a fast control topology in order to have a larger control bandwidth, thus more accuracy, and a less noisy control (since the *local control system*, which has much higher electronic noise, is switched off); on the other hand if the error signal which senses that d.o.f. is noisy and the coupling factor into dark fringe is low it is sufficient and advisable to engage that d.o.f. with a drift control since the narrow frequency band of the control helps in the decoupling of the d.o.f. from the dominant ones.[2]

The design of the control filters for the fast control mode is a very important issue since the low frequency part, below the unitary gain frequency, determines the accuracy of the loop, and the high frequency part determines the noise performance of the loop. The control filter is developed starting from the modeling of the super-attenuator transfer function, from actuator to mirror, which is essentially a double pendulum with resonance frequencies at a few Hz. The control filters have to be designed in order to suppress the mechanical resonances of the suspension and to have a large low frequency gain.

3.1. Control configuration

The angular control system is formed by a complete set of RF error signals used for aligning the mirrors with respect to the beam, plus some reference error signals used to define the beam plane of the interferometer, see Fig. 3. The beam plane has to be defined by pointing the beam on absolute references in three points, by using three angular d.o.f. to fix the beam to the references, while the remaining d.o.f. will be aligned with respect to the beam. The plane of the interferometer was defined using the input mirrors and the Common End d.o.f.

The input mirrors are controlled so that the beam hits the center of the arm cavity terminal mirrors. The error signal is generated by injecting a sinusoidal excitation to the terminal mirrors (with frequencies below the detection range, from 6 to 8 Hz) and evaluating the longitudinal/angular coupling. If the beam is not well centered on the mirrors, the sinusoidal excitation will be present also in the longitudinal error signals. The continuous centering servo, with a bandwidth of ~mHz, applies misalignment corrections to the input mirrors in order to steer the beam on the terminal mirrors and minimize the angular/longitudinal coupling at the excitation frequency, which reduces also the control noise of the arm cavity mirrors.

The Common End alignment is controlled in *fast control mode* by using the DC signal of the suspended quadrant at the BS pick-off (S51).

[2] For example, the Input Beam has been controlled in drift control mode, as it will shown in the next section, since the Input Beam error signal is strongly affected by the Common End mode and since its coupling in the sensitivity is very low.

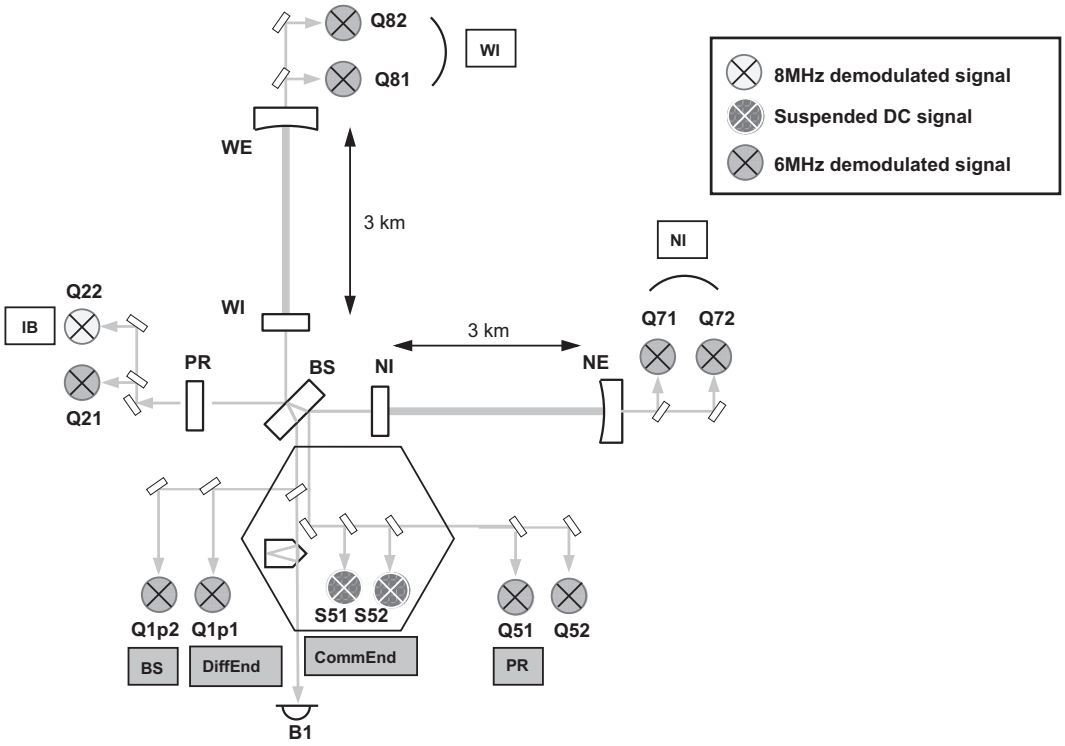

Fig. 3. Configuration of the Automatic Alignment control scheme for the science run VSR2. The schematic shows the signals used to control each d.o.f. (labeled in a gray or white box). The degrees of freedom labeled in gray are controlled by using a fast control topology while the white ones are controlled in drift control mode. For example the Differential End mode is controlled by using the Q1p1 quadrant signal in fast control mode (for the Differential End mode the error signal is extracted at the asymmetric port before the OMC in order to not suppress the higher order modes content) demodulated at ∼6 MHz.

Most of the quadrant diodes are placed on external detection benches since the environmental noises do not couple strongly to the RF signals,[3] as they measure the beat between the sidebands and the carrier. This is not true for the DC signals, which detect the relative position of the quadrant diode with respect to the beam. For this reason in order to have a clean error signal, the environmental noise has to be suppressed by suspending the quadrant in vacuum.

After the plane is defined, the remaining angular degrees of freedom have to be aligned with respect to the main beam. For the angular control two modulation frequencies are used: ∼6 MHz, which is resonating in the central interferometer, and ∼8 MHz which does not enter in the interferometer.

The input beam (IB) is controlled in drift control mode by using the RF signal, demodulated at 8 MHz, reflected by the interferometer (Q22). The two quadrants placed at the dark port, Q1p1 and Q1p2 separated by 90° of Gouy phase, demodulated at 6 MHz, are used to control, in fast control mode, the Differential End and the BS angular displacements.

At last the PR mirror is controlled by using the pick-off beam of the BS mirror demodulated at 6 MHz (Q51) in fast control mode.

4. Performance

The angular control for the Virgo detector was completed in the commissioning period between winter 2004 and the beginning of 2007 [6]; all the angular degrees of freedom were globally controlled, with a *fast* or *drift* control mode, depending on the noise performance of each loop.

The quality of an angular control can be evaluated by: the robustness; the accuracy, thus the total RMS of the mirror angular displacements; and by the control noise performances, corresponding to the noise re-injected to the gravitational wave signal in the detection band (above 10 Hz).

During the first Virgo science run (VSR1) the angular control system was very robust, allowing a duty cycle of more than 80% with the longest locking period of about 94 h. The accuracy of the loops was compliant with the requirements, but the control noise was above the design sensitivity below 20 Hz [4].

From July 7th 2009 to January 2010 the second Virgo science run (VSR2) in coincidence with the two LIGO detectors (HLO in Hanford, WA and LLO in Livingstone, LA – USA each [7]) took place.

The interferometer configuration was improved with respect the first scientific run by increasing the input power from 8 to 17 W to improve the shot noise. A Thermal Compensation System (TCS) was then implemented to reduce the thermal lensing on the input mirrors [8].

The stability and robustness of the Virgo detector was very high, achieving a duty cycle of more than 80% with the longest locking period of 143 h allowing to have: more than 90% of duty cycle for single detector, more than 50% for double coincidence and about 20% for triple coincidence [9]. The duty cycle was mainly limited by maintenance and commissioning periods.[4]

From the point of view of the angular control system, since the accuracy requirements were already fulfilled for VSR1,[5] the commissioning of the automatic alignment system in the period

[3] It has been experienced that the air currents spoil the error signals at low frequency, below ∼1 Hz, but the installation of plexiglass covers on the benches strongly reduced the effect.

[4] The evaluations on the duty cycle and the coincidence periods have been done by simply taking into account the science mode periods for all the three detectors.

[5] The accuracy of the control loops were fulfilling the requirements, being of the order of the nrad for Differential and Common End modes and tens of nrad for the central interferometer d.o.f.

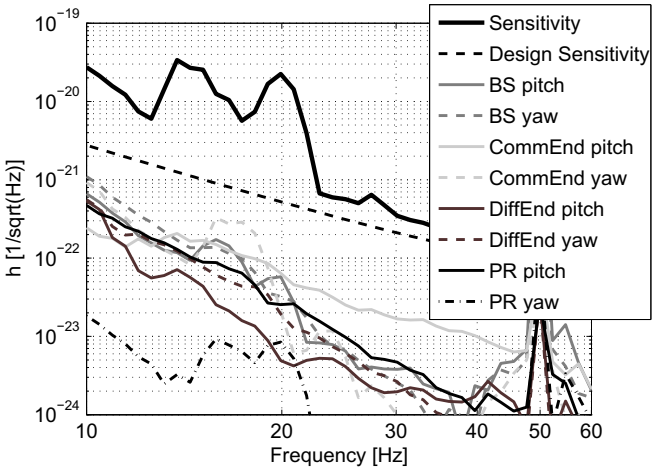

Fig. 4. Noise budget of the Automatic Alignment control system during VSR2 compared to the design sensitivity curve and to the measured sensitivity. The total angular noise is well below the sensitivity curve and below the Virgo design in the whole detection band.

between the two runs was focused to reduce the angular control noise.

Since the unity gain frequency of the fast angular controls is of the order of a few Hz, the noise performance depends on the dark fringe coupling factor, on the high frequency roll-off of the control filters and on the sensing noise (electronic plus shot noise).

In order to reduce the angular control noise contribution to the Virgo sensitivity some improvements to the Automatic Alignment control scheme have been applied.

The sensing noise has been lowered thanks to the implementation of improved demodulator and ADC (analog–digital converter) boards. The new demodulator boards have a lower electronic noise, smaller than the ADC noise, and remotely tunable gain to optimize the signal amplitude at each locking phase. The new ADC boards have smaller non-linearities, with respect to the ones used in VSR1, even if their noise is still dominant for the most critical d.o.f., such as the Differential End and Common End modes.

Rigid plexiglass covers have been installed on the detection benches to reduce the environmental noise, reducing the air currents which affect the error signals in the low frequency region (below a few Hz) spoiling the control accuracy.

Moreover some modifications in the control strategy have been applied, as the use of a second quadrant on the dark fringe beam[6] to sense the BS and the use of the suspended quadrant diode for the Common End mode. Both of these signals have better performances in terms of electronics/shot noise and are less affected by environmental noises.

As a result during VSR2 the angular control noise was below the design sensitivity in the entire detection band, see Fig. 4.

5. Conclusions

During the second Virgo scientific run the angular control was complete, robust and well performing in terms of accuracy and control noise reintroduction in the gravitational wave signals.

The noise performances, with respect to VSR1, were optimized by improving the electronics and the control strategy with respect to the VSR1 scheme, resulting in a control noise below the design sensitivity in the whole detection band.

The system is currently in commissioning phase to fulfill the requirements for the Virgo + configuration, for the third Virgo scientific run (VSR3) which should start at the end of July 2010, which requires better performances in the 10 Hz region. The angular control will be modified to face with the Monolithic Suspensions implementation, whose installation is foreseen at the beginning of 2010, and further improvements on the electronics are planned.

Acknowledgements

The work has been carried out also with support of the Italian Ministero dell'Istruzione, dell'Universita' e della Ricerca through Grant PRIN 2007NXMBHP.

References

[1] T. Accadia et al., Status and perspectives of the Virgo gravitational wave detector, J. Phys. Conf. Ser. 203 (2010) 012074.
[2] F. Acernese et al., Measurements of Superattenuator seismic isolation by Virgo interferometer, Astropart. Phys. 33 (2010) 182–189.
[3] F. Acernese et al., Virgo Collaboration, Lock acquisition of the Virgo gravitational wave detector, Astropart. Phys. 30 (2008) 29–38.
[4] F. Acernese et al., Automatic alignment for the first science run of the Virgo interferometer, Astropart. Phys. 33 (2010) 131.
[5] F. Acernese et al., Virgo Collaboration, A local control system for the test masses of the VIRGO gravitational wave detector, Astropart. Phys. 20 (2004) 617–628.
[6] F. Acernese et al., Virgo Collaboration, The Virgo automatic alignment system, Classical Quantum Gravity 23 (2006) S91–S102.
[7] J.R. Smith et al., LIGO Scientific Collaboration, The path to the enhanced and advanced LIGO gravitational-wave detectors, Classical Quantum Gravity 26 (2009) 114013.
[8] T. Accadia et al., Virgo collaboration, A thermal compensation system for the gravitational wave detector Virgo, in: Proceedings of the 12th Marcel Grossmann Meeting.
[9] Evaluations done by B. Swinkels. Available from: <http://wwwcascina.virgo.infn.it/MonitoringWeb/Inspirals/index.html>.

[6] The second quadrant on the dark fringe (Q1p2) is at 90° of Gouy phase difference with respect to the quadrant used to sense the Differential End mode.